Combustion synthesis and properties of strontium substituted lanthanum manganites $La_{1-x}Sr_xMnO_3$ ($0 \leqslant x \leqslant 0.3$)

Singanahally T. Aruna, Meiyappan Muthuraman and Kashinath C. Patil†

Department of Inorganic and Physical Chemistry, Indian Institute of Science, Bangalore-560 012, India

Strontium substituted lanthanum manganites $La_{1-x}Sr_xMnO_3$ ($x = 0$, 0.1, 0.16, 0.2 and 0.3) have been prepared by a solution combustion process using lanthanum nitrate, strontium nitrate and manganese nitrate as oxidizers and oxalyl dihydrazide as fuel at 300 °C in a pre-heated muffle furnace. As-formed lanthanum manganites are X-ray crystalline showing cubic symmetry. The cubic $LaMnO_3$ with 36% Mn^{4+} changes to a rhombohedral phase ($Mn^{4+} = 28\%$) on calcination at 1000 °C. The surface area and average agglomerated particle size of the as-formed manganites are in the range 12–19 $m^2\ g^{-1}$ and 5.4–8.0 μm, respectively. Sintering, thermal expansion and dc electrical conductivity measurements of $La(Sr)MnO_3$ have been carried out. Strontium substituted lanthanum manganites achieve >80% theoretical density after sintering at 1350 °C for 4 h and the percentage theoretical density decreases with increasing strontium content. The thermal expansion coefficient of $La(Sr)MnO_3$ increases with increasing Sr^{2+} content and $La_{0.84}Sr_{0.16}MnO_3$ shows a highest conductivity value of 202 S cm^{-1} at 900 °C in air.

Solid oxide fuel cells (SOFCs), which operate near 1000 °C offer a clean, pollution-free technology for the electrochemical generation of electricity at high efficiency.[1] The most frequently used SOFC system, employs yttria stabilized zirconia (YSZ) as an electrolyte, cermet like Ni-YSZ as an anode, conducting oxides such as lanthanum manganites, $La_{1-x}M_xMnO_3$ (M = Sr, Ba) or $LaCoO_3$ as cathode and $LaCrO_3$ as interconnect.[1] Among the various cathode materials, the perovskite family lanthanum manganites have been widely studied because of their high electronic conductivity, good chemical stability and thermal expansion compatibility with the solid electrolyte.[2] Lanthanum manganite is a mixed-valence semiconductor containing both Mn^{3+} and Mn^{4+} which is responsible for its electrical conductivity.[3–5] It exhibits phase transformations from orthorhombic to rhombohedral and then to cubic with increasing Mn^{4+} content in the stoichiometry.[4] The Mn^{4+} content in lanthanum manganites can be varied by altering the firing temperature and atmosphere or by the substitution of divalent ions in lanthanum sites.[6,7] $LaMnO_3$ perovskites can tolerate a considerable portion of vacancies in the A site (La site) giving rise to compositions of the type $La_{1-\delta}MnO_3$ with the charge compensated by Mn^{4+} ion formation.[8] Although traditionally lanthanum manganite is considered as an anion excess compound ($LaMnO_{3+\delta}$), detailed investigations by employing high-resolution electron microscopy and other cognate techniques have revealed the presence of metal vacancies ($La_{1-\gamma}Mn_{1-\gamma}O_3$) instead of interstitial oxygen ions.[9,10] A polaron hopping mechanism has been suggested for alkaline-earth substituted $LaMnO_3$ and $LaCrO_3$ with low activation energy and the charge carriers are transported by the $Mn^{3+}—O—Mn^{4+}$ network.[11] From the proposed polaron hopping mechanism, it is evident that maintaining compositional homogeneity within the perovskite lattice is an important criterion for high electrical conductivity, thermal and chemical stability at the working temperature and its compatibility with other components like electrolytes and interconnects of SOFC.[12]

A number of synthetic routes like solid-state,[13] sol–gel,[14] citrate-gel,[15] co-precipitation[6,16] *etc.* have been reported in the literature for the preparation of alkaline-earth substituted lanthanum manganites. In the present study, a simple solution combustion process,[17] has been used to prepare unsubstituted and strontium substituted lanthanum manganites. The solution combustion process is an attractive synthetic route particularly for the preparation of multicomponent oxide materials, since the homogeneity of the aqueous solution of the salts is preserved in the combustion residue. In addition to better homogeneity and purity of the product, the solution combustion method has the advantage of doping desired amounts of impurity ions and a low processing temperature leading to uniform crystalline particle size at superfine dimensions.[17]

The objectives of the present investigation are to study the phase transformation of combustion derived $LaMnO_3$ and to compare its thermal expansion and electrical conductivity with strontium substituted $LaMnO_3$ derived from a solution combustion process. The formal notation, $La(Sr)MnO_3$ is used throughout this article for simplicity. The combustion derived products were characterized by chemical analysis, powder XRD, particle size and surface area measurements. Direct current electrical conductivity and thermal expansion behaviour have been studied on sintered rectangular and cylindrical pellets respectively, in order to check the compatibility of the manganites for SOFC application.

Experimental

Lanthanum nitrate, strontium nitrate and manganese nitrate were used as oxidizers and oxalyl dihydrazide, $C_2H_6N_4O_2$ (ODH) was used as fuel. The oxidizer : fuel ratio was calculated based on oxidizing (O) and fuel (F) valencies of the reactants, keeping O/F = 1, as reported earlier.[18] The aqueous redox solution containing metal nitrates and ODH when introduced into a muffle furnace preheated to 300 °C, boils, froths, ignites and catches fire to give a voluminous combustion residue. The as formed powders were free from any carbon residue.

The compositions of the samples were confirmed by inductively coupled plasma (ICP) atomic emission spectroscopy (Jobin-Yvon Model JY-24). Calcination of the samples was carried out in platinum crucibles at various temperatures, with heating and cooling rates of 10 °C min^{-1} and a soaking period of 2 h. The identification of various phases was carried out using a Shimadzu XD-D1 X-ray diffractometer with Ni-filtered Cu-Kα radiation). The lattice parameters and crystallite sizes were calculated using a least-squares fit method and Scherrer's formula,[19] respectively for the XRD patterns recorded at a scanning rate of 0.5° $2\theta\ min^{-1}$. BET surface areas of the as-formed powders were measured using a Micromeritics Model 2100E Accusorb instrument. Particle size distribution

† E-Mail: kcpatil@ipc.iisc.ernet.in

of the as-formed powders was measured using a SediGraph particle size analyzer (model 5100 V2.03). Microstructures of sintered pellets were studied using a scanning electron microscope (SEM, JEOL model JSM-840A).

The linear thermal expansion of sintered pellets (height 7–8 mm and diameter 9–10 mm) was measured using a home-built dilatometer (with quartz push rod and LVDT setup) in the temperature range 25–900 °C with a heating rate of 2 °C min^{-1}. The dilatometer was calibrated with a NBS reference sapphire (SRM 732). The dc electrical conductivity was measured as a function of temperature on the sintered rectangular specimens (*ca.* $3 \times 3 \times 10$ mm) using a four-probe method. Platinum wires (0.2 mm thick) were used as current and potential leads and the measurements were carried out in the temperature range 25–900 °C with a heating rate of 5 °C min^{-1}. Current and voltage were measured using calibrated multimeters (Mecco, India). Temperature near the sample was measured using a calibrated CrAl thermocouple which was kept within 2–3 mm from the sample and the rate of heating was controlled by a temperature programmer (Century systems, India).

Results and Discussion

Aqueous solutions containing stoichiometric amounts of metal nitrates and ODH, when rapidly heated at 300 °C, undergo dehydration followed by frothing. The decomposition of metal nitrates and ODH starts at one corner and the gaseous products (nitrogen oxides, HNCO, CO and NH_3) which are hypergolic in nature, ignite the mixture. The combustion wave propagates throughout the reaction mixture without further need of external heating as the energy released during combustion is more than the heat required for the decomposition of the redox mixture. The flame temperature, measured by inserting a thermocouple was 900 ± 50 °C which persists for a few minutes. The formation of $LaMnO_3$ by the combustion reaction can be represented by the reaction

$$4\ La(NO_3)_{3\ (aq)} + 4\ Mn(NO_3)_{2\ (aq)} + 10\ C_2H_6N_4O_{2\ (aq)} + O_{2\ (g)} \rightarrow 4\ LaMnO_{3\ (s)} + 20\ CO_{2\ (g)} + 30\ H_2O_{\ (g)} + 30\ N_{2\ (g)}$$

The atmospheric oxygen oxidizes Mn^{2+} to Mn^{3+}/Mn^{4+} during the combustion. The La : Sr : Mn ratios in $La(Sr)MnO_3$ as determined by ICP analysis are listed in Table 1. The atomic ratio of La, Sr and Mn in the combustion product are in agreement with the starting composition taken for combustion synthesis.

Powder characterization

As-formed lanthanum manganites are found to be X-ray crystalline, corresponding to cubic symmetry. The strong oxidizing atmosphere which exists during combustion reaction of the redox mixture leads to excess Mn^{4+} in the $LaMnO_3$ structure and thus stabilizes the cubic phase.[5] Also the quenching of the product from the flame temperature (*ca.* 900 °C) to room temperature appears to favour the stabilization of Mn^{4+}. The Mn^{4+} content in the as-formed $LaMnO_3$ was 36% as estimated from iodimetry.[13] Calcination of as-formed $LaMnO_3$ at 700 °C stabilized the cubic phase. On further calcination at 1000 °C, the Mn^{4+} content decreases to 28% and the phase changes to rhombohedral (Fig. 1). As-formed $La_{1-x}Sr_xMnO_3$ also shows a cubic phase and the lanthanum manganites with $x < 0.3$ change to rhombohedral ($Mn^{4+} \approx 24\%$) after calcination at 1350 °C for 2 h (Fig. 2). $La_{1-x}Sr_xMnO_3$, with $x = 0.3$ when calcined at 1350 °C shows a cubic phase with 44% Mn^{4+} [Fig. 2(*e*)]. The stabilization of rhombohedral and cubic phases in $La(Sr)MnO_3$ at higher temperatures is due to the substitution of Sr^{2+} in La^{3+} sites resulting in higher Mn^{4+} content.[13]

It has been reported[20–22] that $LaMnO_3$ undergoes a phase transformation from orthorhombic to rhombohedral and then to cubic with increasing concentration of Mn^{4+} on calcination in an oxygen atmosphere or by electrochemical oxidation. The formation of an orthorhombic phase at lower Mn^{4+} (< 12%) content has been attributed to the Jahn–Teller ordering of four coplanar empty orbitals of Mn^{3+} ions.[23,24] The combustion derived $LaMnO_3$ always contains > 20% Mn^{4+} and the orthorhombic phase was not observed in any of the samples. The lattice parameter calculations from the XRD patterns of the sintered (1350 °C) samples (Table 2) show that the rhombohedral unit-cell dimension (a_r) decreases with increasing

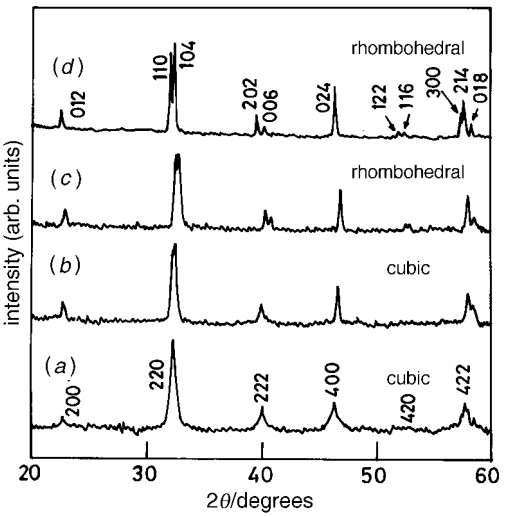

Fig. 1 Powder XRD patterns (Cu-Kα) of as-formed and calcined $LaMnO_3$: (*a*) as prepared, (*b*) 700 °C, (*c*) 1000 °C and (*d*) 1350 °C

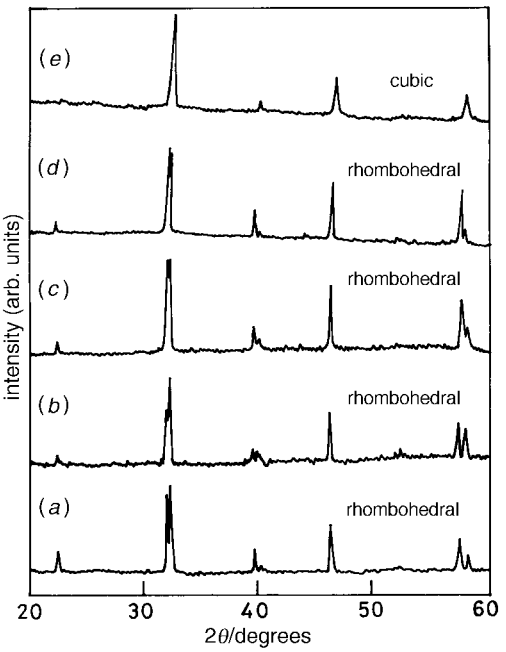

Fig. 2 Powder XRD patterns (Cu-Kα) of $La_{1-x}Sr_xMnO_3$ calcined at 1350 °C, 4 h: (*a*) $x = 0$, (*b*) $x = 0.1$, (*c*) $x = 0.16$, (*d*) $x = 0.2$ and (*e*) $x = 0.3$

Table 1 Chemical analysis of $La_{1-x}Sr_xMnO_3$ (in terms of atomic ratio)

x	La	Sr	Mn
0	0.980	—	1.000
0.1	0.893	0.104	1.000
0.16	0.832	0.162	1.000
0.2	0.796	0.213	1.000
0.3	0.722	0.305	1.000

Table 2 Properties of sintered La(Sr)MnO_3 (1350 °C, 4 h)

composition	phase (from XRD)	lattice parameters	thermal expansion coefficient at 900 °C/K^{-1}	conductivity at 900 °C/S cm^{-1}	activation energy/eV
$LaMnO_3$	rhombohedral	$a=5.5318$ Å, $\alpha=60.615°$	11.33	103	0.164
$La_{0.90}Sr_{0.10}MnO_3$	rhombohedral	$a=5.5258$ Å, $\alpha=60.516°$	12.18	166	0.155
$La_{0.84}Sr_{0.16}MnO_3$	rhombohedral	$a=5.4893$ Å, $\alpha=60.41°$	12.63	202	0.084
$La_{0.80}Sr_{0.20}MnO_3$	rhombohedral	$a=5.4734$ Å, $\alpha=60.30°$	13.13	155	0.090
$La_{0.7}Sr_{0.3}MnO_3$	cubic	$a=7.7611$ Å	13.74	144	0.100

strontium substitution in $LaMnO_3$. This may be due to the increase in the concentration of smaller Mn^{4+} ions compared with Mn^{3+} ions in La(Sr)MnO_3 which results in unit cell contraction.[24]

Particulate properties of as-formed $LaMnO_3$ and La(Sr)MnO_3 are summarized in Table 3. The crystallite sizes calculated from the XRD line broadening using Scherrer's formula[19] are in the range 13–19 nm. However, as-formed lanthanum manganites are weakly agglomerated with an average agglomerated particle sizes of 5.4–8.0 μm. This may be attributed to the high *in situ* combustion temperature which tends to agglomerate the primary particles to some extent. Mechanical milling of the powder for 30 min reduces the agglomerated size to *ca.* 1.5 μm. The particle size distributions of as-formed and milled $LaMnO_3$ are shown in Fig. 3. The surface areas of the manganites are in the range 12–19 $m^2\ g^{-1}$ and the grinding does not have an effect on the surface area. This suggests that the as-formed powders are porous and the pore surfaces also contribute to the specific surface area of the samples.

Sintering, thermal expansion and electrical conductivity studies

The combustion derived powders were crushed and uniaxially pressed (50 MPa) into compacts using poly(vinyl alcohol) (5% aqueous solution) as a binder. The binder was removed by heating the pellets at 700 °C for 30 min. Sintering of the pellets was carried out at 1350 °C in air with a heating rate of 10 °C min^{-1} and soaking for 4 h. The bulk density and open porosity of the sintered pellets were measured using

Table 3 Powder properties of as-formed La(Sr)MnO_3

composition	surface area/$m^2\ g^{-1}$	average aggregate particle size/μm	crystallite size/nm
$LaMnO_3$	12	5.41	14.0
$La_{0.90}Sr_{0.10}MnO_3$	13	6.22	19.3
$La_{0.84}Sr_{0.16}MnO_3$	15	7.30	16.5
$La_{0.80}Sr_{0.20}MnO_3$	17	7.45	14.7
$La_{0.7}Sr_{0.3}MnO_3$	19	8.05	13.3

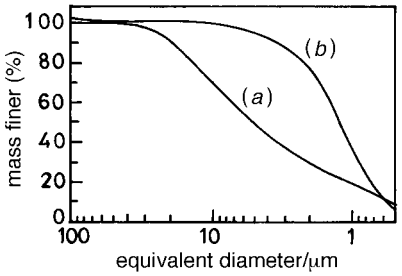

Fig. 3 Particle size distribution of as-formed [(*a*), median diameter 5.41 μm] and milled [(*b*), median diameter 1.28 μm] $LaMnO_3$

Archimedes liquid displacement technique. The sintered density achieved was >80% theoretical density in all the cases and was higher at lower substitution level. The dominating effect in the sintering behaviour of La(Sr)MnO_3 is cationic diffusion and other effects like gas- or liquid-phase diffusion are less likely, since the melting point of La(Sr)MnO_3 is rather high and none of the constituent oxides are known to be volatile.[25] The main influence on ionic diffusion depends on (*i*) powder morphology, (*ii*) the difference in ionic radii between lanthanum and strontium and (*iii*) the number of vacancies in La(Sr) sites.[25] Thus, the poor sintering in strontium substituted manganites has been attributed to the higher agglomerated particle size of strontium substituted manganite powders. Also, the combined effect of the difference in ionic radii between La^{3+} and Sr^{2+} and the decrease in the number of defects that are formed in La(Sr)MnO_3 with increasing strontium content appears to be responsible for the difference in the sintering behaviour.[25] The microstructure of strontium substituted lanthanum manganites sintered at 1350 °C (Fig. 4) shows the porous nature of the sintered body and the SEM image of the fracture surface reveals that the pores are interconnected.

Plots of thermal expansion *vs.* temperature of $La_{1-x}Sr_xMnO_3$ ($x=0$, 0.16, 0.3) sintered at 1350 °C for 4 h are shown in Fig. 5. The thermal expansion coefficients, α (Table 2) increase with increasing substitution of strontium. At lower substitution levels the α value is close to that of yttria stabilized zirconia ($11.5\times10^{-6}\ K^{-1}$),[25] the electrolyte of SOFC.

Lanthanum manganite is a p-type semiconductor and the conductivity is essentially due to the hole motion in the d electron energy levels of manganese.[7] The temperature dependence of resistivity (ρ) of $LaMnO_3$ and La(Sr)MnO_3 is shown in Fig. 6. At lower levels of Sr^{2+} ion substitution in lanthanum sites ($x\leqslant0.1$), semiconductor-like behaviour is observed in the temperature range investigated, *i.e.* the resistivity decreases with increasing temperature. At higher Sr^{2+} concentrations, $x\geqslant0.16$, metallic behaviour, *i.e.* increase in resistivity with temperature, was observed at low temperatures. After a particular temperature (T_t) it behaves as a typical semiconductor and this transition temperature coincides with the ferromagnetic T_c of the material.[21] The increase in resistivity below a certain temperature (T_c) is typical behaviour for a degenerate semiconductor,[27] and above T_c the resistivity decreases with temperature. The resistivity behaviour below T_c, could be ascribed to the transport of holes in an extended band and above T_c to the hopping motion of localized holes.[27]

The electrical conductivity and activation energy for conduction are summarized in Table 2. The plot of $\log(\sigma T)$ *vs.* $1/T$ of $La_{1-x}Sr_xMnO_3$ with $x<0.16$ is linear in the measured temperature range and for $x\geqslant0.16$ it is linear above the transition temperature (T_t). The linear dependence of $\log(\sigma T)$ *vs.* $1/T$ (Fig. 7) is characteristic of the polaron hopping transport mechanism[28] for which the conductivity can be represented by the function $\sigma=(A/T)\exp(-E_a/kT)$. It has been reported that a transition in conductivity occurs in unsubstituted lanthanum manganite sintered above 1200 °C due to the orthorhombic to

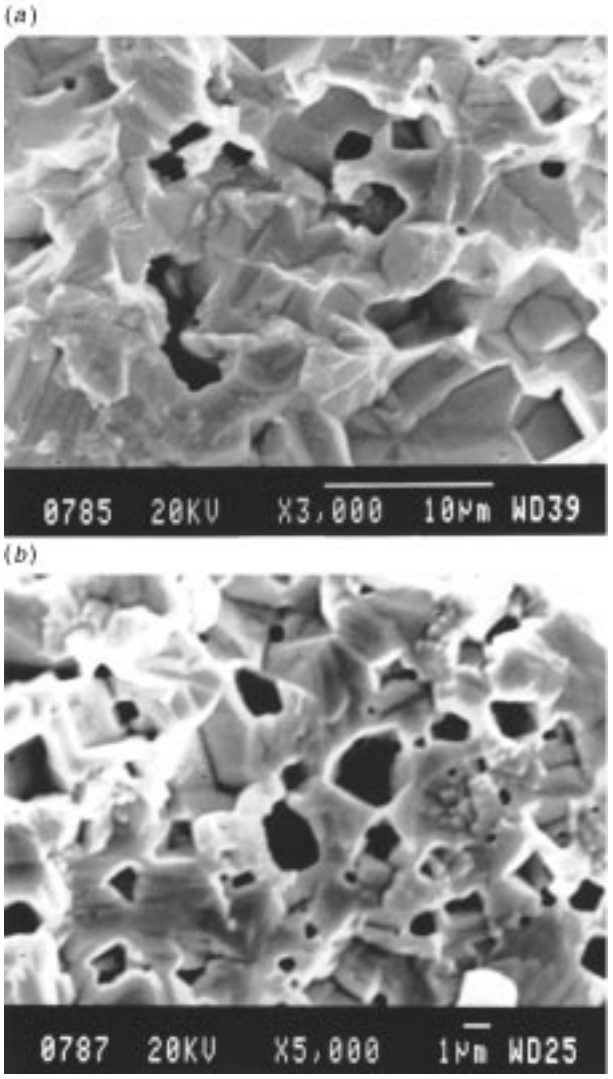

Fig. 4 Scanning electron micrographs of $La_{0.84}Sr_{0.16}MnO_3$ sintered at 1350 °C, 4 h at low (*a*) and high (*b*) magnifications

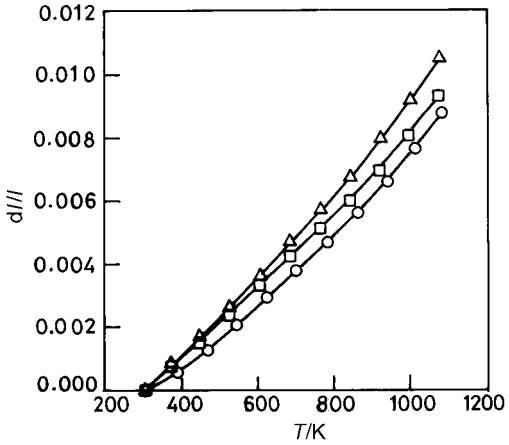

Fig. 5 Thermal expansion of the sintered samples of $La_{1-x}Sr_xMnO_3$ [$x=0$ (○), 0.16 (□) and 0.3 (△)]

rhombohedral phase transition and the transition temperature decreases with increasing Mn^{4+} content.[5,29] However, no transition in conductivity was observed for the unsubstituted combustion derived lanthanum manganite sintered at 1350 °C (Fig. 7), which may be attributed to the presence of rhombohedral structure at room temperature (Fig. 2).

The activation energy (E_a) for electrical conduction calcu-

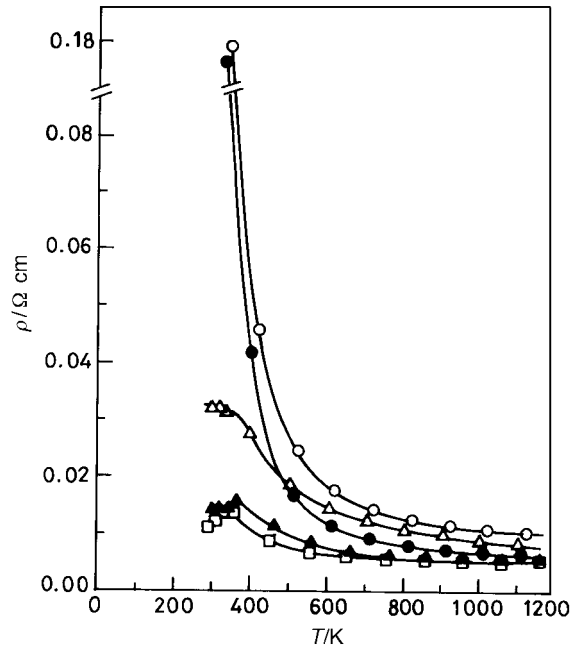

Fig. 6 Resistivity *versus* temperature plot of $La_{1-x}Sr_xMnO_3$ [$x=0$ (○), 0.1 (●), 0.16 (□), 0.2 (▲) and 0.3 (△)] sintered at 1350 °C for 4 h

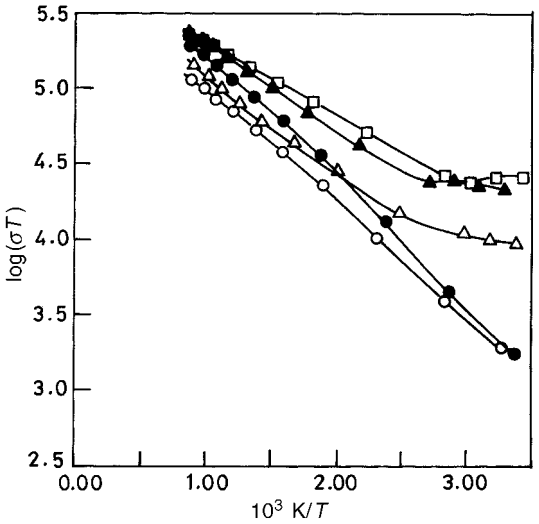

Fig. 7 Electrical conductivity (σ) of $La_{1-x}Sr_xMnO_3$ [$x=0$ (○), 0.1 (●), 0.16 (□), 0.2 (▲) and 0.3 (△)] sintered at 1350 °C for 4 h, represented as $\log(\sigma T)$ *versus* reciprocal temperature

lated from the slope of $\log(\sigma T)$ *vs.* $1/T$ decreases with increasing strontium substitution (Table 2). The decrease in activation energy may be attributed to the increase in the Mn^{4+} content which reduces the Mn—Mn distance and brings the Mn—O—Mn angle closer to 180°.[29] However, there is a slight increase in the activation energy above $x=0.16$. The conductivity value at 900 °C increases with increasing substitution of strontium to $x=0.16$ above which it started decreasing. The decrease in conductivity and increase in the activation energy at higher substitution level may be due to the decrease in sintered density as the electrical conductivity is known to depend on the microstructure and density.[12] $La_{0.84}Sr_{0.16}MnO_3$ shows highest conductivity of 202 S cm^{-1} at 900 °C in air which is higher than that reported by Kertesz *et al.* for the same composition (190 S cm^{-1}) having the theoretical maximum density.[12] The higher conductivity may be due to a combination of surface and grain boundary effects as well as higher Mn^{4+} content. Also, the good contacts between grains

and the interconnected pores in the sintered body (Fig. 4) may be responsible for the higher conductivity observed.

Conclusions

Unsubstituted and strontium substituted lanthanum manganites have been successfully prepared by a low-temperature initiated solution combustion process using the corresponding metal nitrates and oxalyl dihydrazide. On calcination the Mn^{4+} content in $LaMnO_3$ decreases and correspondingly the crystallographic phase transforms from cubic to rhombohedral. In the case of strontium substituted lanthanum manganites the rhombohedral or cubic phase is stabilized even after calcination at higher temperature (1350 °C) depending on the strontium content. The thermal expansion coefficient (α) of $LaMnO_3$ is 11.33×10^{-6} K^{-1}, and the α value increases with increasing strontium substitution. The electrical conductivity in $La_{1-x}Sr_xMnO_3$ increases up to $x=0.16$ above which it decreases. A highest conductivity of 202 S cm^{-1} was observed for $La_{0.84}Sr_{0.16}MnO_3$ at 900 °C in air, with a sintered density 90% of the theoretical value.

The authors would like to thank Mr. Nagesh kini for thermal expansion measurements and Dr. N. Munichandraiah for useful discussions. One of the authors (S.T.A.) thanks the CSIR, New Delhi for a Junior Research Fellowship. Financial support from the Ministry of Non-conventional Energy Sources, New Delhi is gratefully acknowledged.

References

1 N. Q. Minh, *J. Am. Ceram. Soc*., 1993, **76**, 563.
2 A. Hammouche, E. Siebert and A. Hammou, *Mater. Res. Bull*., 1989, **24**, 367.
3 K. Kamata, T. Nakajuma, T. Hayashi and T. Nakamura, *Mater. Res. Bull*., 1978, **13**, 49.
4 G. V. Subbarao, B. M. Wanklyn and C. N. R. Rao, *J. Phys. Chem. Solids*, 1971, **32**, 345.
5 G. H. Jonker, *J. Phys. Chem. Solids*, 1959, **9**, 165.
6 D. W. Johnson Jr, P. K. Gallagher, F. Schrey and W. W. Rhodes, *Am. Ceram. Soc. Bull*., 1976, **55**, 520.
7 G. H. Jonker and J. H. Van Santen, *Physica*, 1950, **16**, 599.
8 V. Ferris, L. Brohan, M. Ganne and M. Tournoux, *Eur. J. Solid State Inorg. Chem*., 1995, **32**, 131.
9 M. Hervieu, *Eur. J. Solid State Chem*., 1995, **32**, 79.
10 J. A. M. van Roosmalen and E. H. P. Cordfunke, *J. Solid State Chem*., 1994, **110**, 106.
11 J. H. Kuo, H. U. Anderson and D. M. Sparlin, *J. Solid State Chem*., 1990, **87**, 55.
12 M. Kertesz, I. Riess, D. S. Tannhauser, R. Langpage and F. J. Rohr, *J. Solid State Chem*., 1982, **42**, 125.
13 G. H. Jonker and J. H. Van Santen, *Physica*, 1950, **16**, 377.
14 H. Taguchi, D. Matsuda, M. Nagao, K. Tanihata and Y. Miyamoto, *J. Am. Ceram. Soc*., 1992, **75**, 201.
15 M. S. G. Baythoun and F. R. Sale, *J. Mater. Sci*., 1982, **17**, 2757.
16 S. A. Prokudina, Ya. S. Rubinchik and M. M. Pavlyuchenko, *Inorg. Mater*., 1974, **10**, 416.
17 K. C. Patil, *Bull. Mater. Sci*., 1993, **16**, 533.
18 S. S. Manoharan and K. C. Patil, *J. Solid State Chem*., 1993, **102**, 267.
19 H. Klug and L. Alexander, *X-ray Diffraction Procedures*, John Wiley, New York, 1962.
20 M. Verelst, N. Rangavittal, C. N. R. Rao and A. Rousset, *J. Solid State Chem*., 1993, **104**, 74.
21 R. Mahendiran, R. Mahesh, A. K. Raychaudri and C. N. R. Rao, *Pramana J. Phys*., 1995, **44**, 393.
22 R. Mahesh, K. R. Kannan and C. N. R. Rao, *J. Solid State Chem*., 1995, **114**, 294.
23 A. Wold and R. J. Arnott, *J. Phys. Chem. Solids*, 1959, **9**, 176.
24 B. C. Tofield and W. R. Scott, *J. Solid State Chem*., 1974, **10**, 183.
25 J. A. M. van Roosmalen, E. H. P. Cordfunke and J. P. P. Huijsmans, *Solid State Ionics*, 1993, **66**, 285.
26 T. Ishihara, T. Kudo, H. Matsuda and Y. Takita, *J. Am. Ceram. Soc*., 1994, **77**, 1682.
27 J. Tanaka, M. Umehara, S. Tamura, M. Tsukioka and S. Ehara, *J. Phys. Soc. Jpn*., 1982, **51**, 1236.
28 D. P. Karim and A. T. Aldred, *Phys. Rev. B*, 1979, **20**, 2255.
29 J. A. M. van Roosmalen, J. P. P. Huijsmans and L. Plomp, *Solid State Ionics*, 1993, **66**, 279.

Paper 7/03901H; *Received* 4*th June*, 1997